7.1 Introduction

Bioactive glasses were discovered in 1969 first time as an alternative, second-generation interfacial bonding of an implant with host tissues. Bioglass®45S5 developed by Hench and co-workers (Hench et al. 2006) consisting of 45 wt.% SiO_2, 24.5 wt.% Na_2O, 24.5 wt.% CaO, and 6 wt.% P_2O_5 has been found to be one of the most bioactive glasses. Bioglass®45S5 has higher bone forming ability than synthetic hydroxyapatite due to rapid surface reactions within the body (Oonishi et al. 1999; 2000).

Hydroxyapatite ($Ca_{10}(PO_4)_6(OH)_2$) has a similar chemical and crystallographic structure like bone mineral. Extensive studies have indicated that HA exhibits osteoconductive properties and it is biocompatible with hard tissues of human beings (Elliott et al. 1973; Hong et al. 1992; Edwards et al. 1997). However, during applications of load-bearing implants its poor mechanical properties are the most serious obstacles. Hydroxyapatite HA, bioglass (BG) are biocompatible ceramic materials commonly used as substitutes in orthopedics, dentistry, maxillofacial surgery, and tissue engineering as it can promote favorable bone tissue formation. Some previous works indicated that if bioglass is added to pure hydroxyapatite, it showed poor mechanical properties but improved its biological properties (Kleebe et al.1997).

On the other hand, for load-bearing implants, mechanical properties of titania and its alloys are good enough, but their biocompatibility is much worse than that of calcium phosphate ceramics (Healy et al. 1992). But significant differences in physical and thermal properties between titania and hydroxyapatite inevitably limit the use of this kind of materials (Jansen et al. 1991). By powder metallurgy method titania /

hydroxyapatite biocomposites were made from hydroxyapatite, titania powders to combine the bioactivity of hydroxyapatite and the mechanical properties of titania. For the material used as an implant in a human body, the sintering additive should be nontoxic, having good biocompatibility and provide sufficient mechanical strength to the sintered material. Due to increased biocompatibility and decreased yield strength, many research has focused on β-Ti alloys. While it is generally considered that Ti and Ti alloys are bioinert so these metallic materials cannot bond directly to bone tissue because this is an inorganic/organic (ceramic–polymer) composite. Therefore, various surface modifications have been carried out on Ti implants to improve their bioactivity (Kim et al. 2012). Among these surface modifications, hydroxyapatite has been frequently deposited on Ti implants to improve the cell responses, osteoconductivity because of its similarity in composition and crystal structure to bone minerals, which have been considered to be Ca-deficient apatites with substituted elements (Lee et al.2010).

The niobium (Nb) is a non-toxic element (Dsouki et al. 2014) used in implants due to its excellent corrosion resistance, good biological compatibility in soft and hard tissues. A compact barrier type oxide layer (niobium pentoxide) tightly covers the entire metal surface due to biocompatibility and corrosion resistance. bone-bond ability (osseointegration) is another key point to extend the implants lifetime. When implanted in osseous tissue, the bone-bonding mechanism depends on the surface topography (Gupta et al. 2000), porosity, wettability (Bacakova et al. 2011) and spontaneous formation of a bone-like apatite layer on the bioactive material (Kokubo et al. 2006). Niobium requires a suitable surface treatment like the sol-gel process to achieve osseointegration similar to titanium. Niobium is a transition metal and has the atomic

number 41. This metal is widely used to enhance mechanical properties in the development of metal alloys. Niobium pentoxide (Nb_2O_5) has shown bioactive properties, like hydroxyapatite crystal growth when comes in contact with human saliva and has been used as an anti-allergic coating in endoprostheses with favorable results (Karlinsey et al. 2006). Therefore, it is used as an alternative for composite development.

Because of its strength, comparatively low stiffness, light weight and bioinertness, commercially pure titania is widely used biomaterial in oral implantology (Kong et al. 2002). When compared to non-coated implants, HA-coated implants have higher integration rate, faster bone attachment and direct bone bonding (Baltag et al. 2000). Long-term animal studies and clinical trials of load-bearing dental and orthopedic prostheses showed that HA coatings degrade with time, and depends upon the degree of crystallinity of the HA. When compared with HA, the glass reinforced HA composites (Bonelike\coating) shows better characteristics for bone cell growth and function.

Titanium is widely used as an artificial implant including dental implants, mini-implants, hip joint, and cranial implants, etc. Among them, β-type Ti-Nb binary alloy is one of the promising implant alloys for biomedical applications as it has certain advantages like good workability, high strength, superior biocompatibility without toxicity metallic ions released (such as Al and V elements) and excellent in vivo osseointegration characteristics. While the microstructures, anticorrosion performances and mechanical properties of the Ti-Nb binary alloys are sensitive to their Nb contents (Lee et al. 2002).

Also, niobium more effectively improves the chemical durability than titanium because of the function of niobium as a glass network former in the $Na_2O–Al_2O_3–TiO_2–Nb_2O_5–P_2O_5$ glass system. It has been proposed that by adding Nb_2O_5, the dissolution rate is well controlled in $Nb_2O_5–SrO–P_2O_5$ glass. The addition of niobium ions into calcium phosphate glasses will play an important role in controlling the material structure and solubility. The effect of adding Nb_2O_5 to calcium phosphate glasses on their structure and physicochemical properties were examined.

7.2. Materials and methods

7.2.1 Preparation of Biocomposites

Biocomposite was prepared by using a mixture of bioglass (45S5), HA, TiO_2 and Nb_2O_5 powders after 45 min of ball milling at 300 rpm rotation speed of ball mill, using 8 balls with the diameter of 20 mm and the ball-to-powder weight (B/P) ratio equal to 35:1. At an applied pressure of 60 MPa, the milled powders were placed in a high chrome high carbon steel die (100mm×60mm×40mm) and compacted by a uniaxial hydraulic press. By using Muffle furnace, the green compacts pellets were sintered at 1100°C in a 10-3 torr vacuum chamber. The sintered biocomposites were cooled in air and the thermocouple is used to measure the temperature of the compacted powders in the sintering process. The composition of bioglass 45S5 and biocomposite samples are shown in Table 7.1.

Table 7.1: Composition of Bioglass and Biocomposites (BGHATiNb1, BGHATiNb2, BGHATiNb3, BGHATiNb4).

Sample	**Composition (wt %)**			
BG (45S5)	45 SiO_2	24.5 Na_2O	24.5 CaO	6 P_2O_5
Biocomposite Samples	**BG (45S5)**	**HA**	**TiO_2**	**Nb_2O_5**
BGHATiNb1	45	5	45	5
BGHATiNb2	40	10	40	10
BGHATiNb3	30	20	30	20
BGHATiNb4	25	25	25	25

The results suggested that there was a possibility of inter diffusion between HA and Ti during sintering (Nath et al. 2009) and the possible reactions could be expressed by the following Eqs. (7.1)–(7.5).

$$Ca_{10}(PO_4)_6(OH)_2 \longrightarrow Ca_{10}(PO_4)_6(OH)_{2-X} + XH_2O \quad \text{-----(7.1)}$$

$$Ti + 2H_2O(gas) \longrightarrow TiO_2 + 2H_2 \quad \text{------(7.2)}$$

$$Ca_{10}(PO_4)_6(OH)_2 + TiO_2 \longrightarrow Ca_3(PO_4)_2 + CaTiO_3 + H_2 + 1/2O_2 \quad \text{------(7.3)}$$

$$Ca_3(PO_4)_2 + 1/2O_2 + 3Ti \longrightarrow 3CaTiO_3 + 2P \quad \text{------(7.4)}$$

$$xTi + yP \longrightarrow Ti_xP_y \quad \text{-------(7.5)}$$

7.3. Results and Discussion

7.3.1 Differential thermal analysis (DTA) / Thermogravimetry Analysis (TGA)

Fig.7.1 explain the thermal analysis (Thermogravimetric TG curve and Differential Scanning Calorimetry DSC) curve of BGHATiNb4 respectively. Three main steps were

observed in the TG curve of BGHATiNb4 biocomposite. The first region shows a decrease in mass ranges from 40 to 200°C with a mass loss of approximately 0.12% which was due to the evaporation of water physically adsorbed on the surface of HA. The second region starts at the temperature of about 200°C and ends at 600°C with a corresponding mass loss of approximately 0.16% which is attributed to the removal of chemically adsorbed water that is irreversible. Endothermic and exothermic events take place at 402°C and 714°C. However, the exothermic broad band dominates the DSC curve which corresponds to a structural rearrangement on the crystal lattice as detected by XRD. By maintaining the heating process, the CO32- that occupies the hydroxide or phosphate sites can be released at the temperature of approximately 700°C without considerable mass loss. There is a reduction of mass 0.71% of the biocomposite powder sample due to the gradual dehydration of hydroxyapatite with the release of hydroxyls at the temperatures above 800°C (Gross et al. 1998).

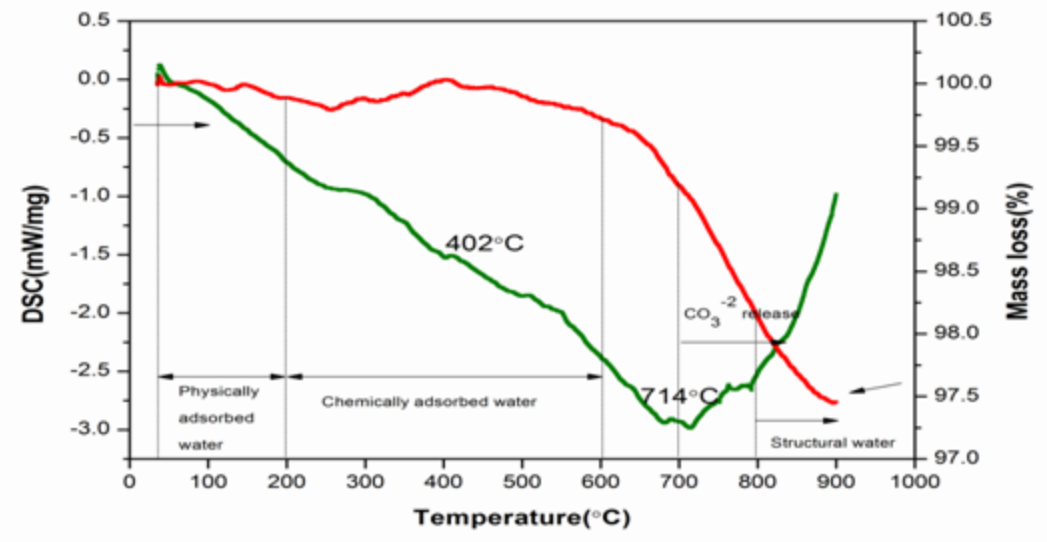

Figure 7.1 The thermal analysis (Thermogravimetric TG curve and Differential Scanning Calorimetry DSC curve of BGHATiNb4 biocomposite.

7.3.2 X-ray diffraction

The XRD pattern of biocomposite sample BGHATiNb1, BGHATiNb2, BGHATiNb3, BGHATiNb4 were presented in Fig.7.2. Crystalline phases were obtained on the surface of biocomposites before and after soaking in SBF for various time periods 1,3,7,14,21 days respectively. After immersion in SBF, crystalline new peaks HA, Nb_2O_5, $CaTiO_3$ appeared in the XRD pattern. These HA react with TiO_2 during the sintering process. (Ning et al. 2004) and (Zhu et al. 2008) studied the reactions in the BGHATiNb sintered composites and suggested that HA would decompose when it was sintered at 1000°C because the sintered temperature is controlled at 1100°C. Initially, hydroxyapatite (HA) peaks developed at (2θ) values of (22°-48°) after three days of soaking in SBF and Nb_2O_5 peaks developed at (2θ) values of (23°-47°) after seven days of immersion. Main crystalline phases of these biocomposites are HA, Nb_2O_5, $CaTiO_3$ JCPDS Card No. (98-000-6285), (98-005-6144), (98-006-6605) respectively.

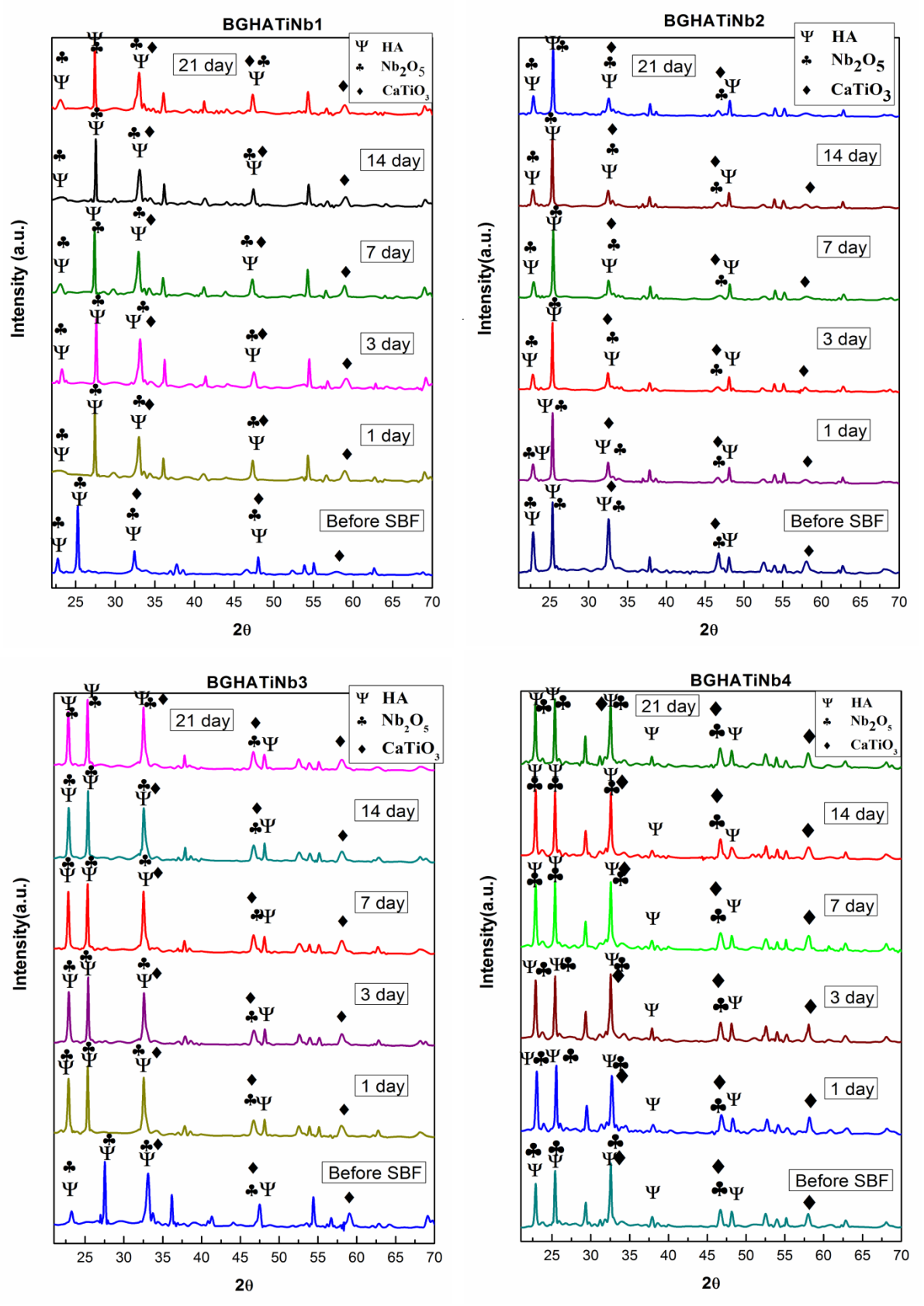

Figure 7.2 XRD analysis of BGHATiNb1, BGHATiNb2, BGHATiNb3, BGHATiNb4 biocomposite before and after immersion in SBF.

7.3.3. Fourier Transform Infrared spectroscopy analysis

Fourier Transform Infrared spectroscopy was used to examine the precipitation that formed on the surface of the composite. Fig. 3(a) shows the FTIR spectra of the precipitation. The bands at 569 and 691 cm^{-1} are caused by phosphate (Li et al. 1994; Bayraktar et al. 1999). The OH- stretching vibration is observed at 3685 cm^{-1}, which is overlapped more or less by the dispersive band of water at 3000 to 3700 cm^{-1}. The strong absorption band at 1491 cm^{-1} and the sharp band at 915, 1684 cm^{-1} are attributed to carbonate absorption which reveals that carbonate ions are present in the structure of the apatite that formed on the surface of the biocomposite. Similar bands are shown in Table 7.2 and Fig. 7.3 for BGHATiNb2, BGHATiNb3 and BGHATiNb4 biocomposite.

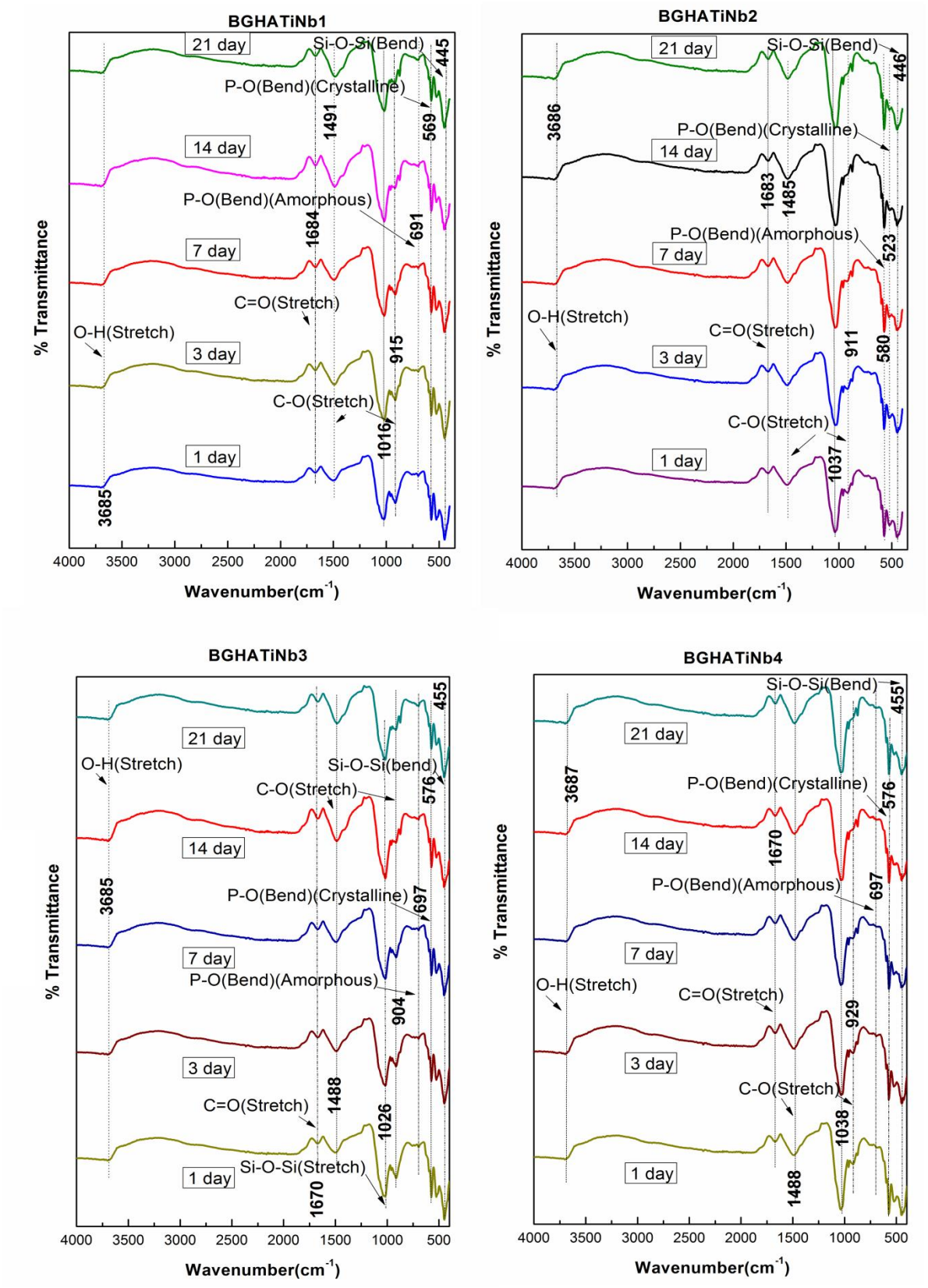

Figure 7.3 FTIR Analysis of BGHATiNb1, BGHATiNb2, BGHATiNb3, BGHATiNb4 biocomposite after immersion in SBF.

Table 7.2: FTIR spectra bands of BGHATiNb1, BGHATiNb2, BGHATiNb3, BGHATiNb4 sample.

Sample	P–O (crystalline)	P–O (amorphous)	C–O (Stretch)	C=O (Stretch)	O–H groups
BGHATiNb1	569	691	915, 1491	1684	3685
BGHATiNb2	523	580	911, 1485	1683	3686
BGHATiNb3	576	697	904, 1488	1670	3685
BGHATiNb4	576	697	929, 1488	1670	3687

7.3.4 pH measurement

By immersing sample in SBF, the in-vitro bioactivity of a biocomposite can be easily predicted which possesses a similar ionic concentration as human blood plasma and thus it can simulate the microenvironment of a bone inside the body (Kokubo et al. 2006). Fig. 7.4 describes the pH of SBF at 1,3, 7, 14 and 21 days. The starting pH of SBF was set to 7.4. The pH of SBF solution rapidly increased within 14 days of incubation followed by a slow decrease. The rapid increase of pH on 14 days mainly occurred at high concentrations of Na^+ and Ca^{2+} ions into SBF solutions by dissolution. A fall of pH was observed after 14 days. There is the decrease in pH due to the release of the hydroxyl radical from the material surface. When the pH value of the physiological solution was over 7.4, CaP compounds were precipitated spontaneously. During the prolonged immersion time, Ca and P ions are consumed largely due to the formation of abundant apatite and simultaneously OH^- is consumed correspondingly. Thus the pH value of SBF decreases (Fan et al. 2009).

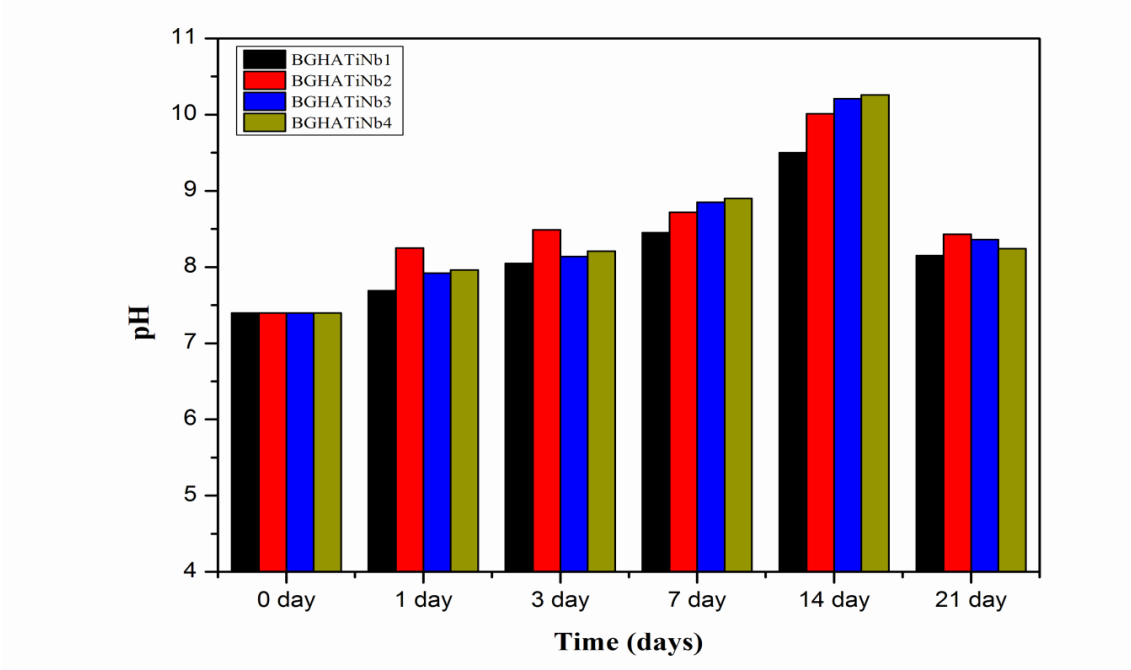

Figure 7.4 pH measurement of BGHATiNb1, BGHATiNb2, BGHATiNb3, BGHATiNb4 biocomposite sample before and after immersion in SBF.

7.3.5 SEM and EDS Analysis of bioomposites

Fig. 7.5(a), (b) shows SEM micrographs of the HA films deposited on the BGHATiNb before and after SBF. The surfaces of BGHATiNb1, BGHATiNb2, BGHATiNb3, BGHATiNb4 biocomposite after SBF were partially covered with an HA layer as shown in Fig.7.5(b). As the Nb concentration increased, agglomerate precipitates were formed for BGHATiNb4. Fig.7.5(b) showed the surface morphologies of the biocomposite after various incubation periods in SBF. These images clearly confirmed apatite formation. After seven days of incubation, BGHATiNb (1-4) showed confluent agglomerate shaped apatite formation. It is evident that the HA nucleation and growth processes were strongly influenced by the amount of Nb and titanium. For the bulk surface of the BGHATiNb, HA nuclei formed at β phase sites, grew rapidly and spread with diminishing surface energy assuming the agglomerate morphology. As shown in Fig. 7.5(c) the EDS results show that all of the surface regions containing HA layers

were composed of Ca, P, Ti, Nb with overall compositions in good agreement with the nominal compositions of HA and titania.

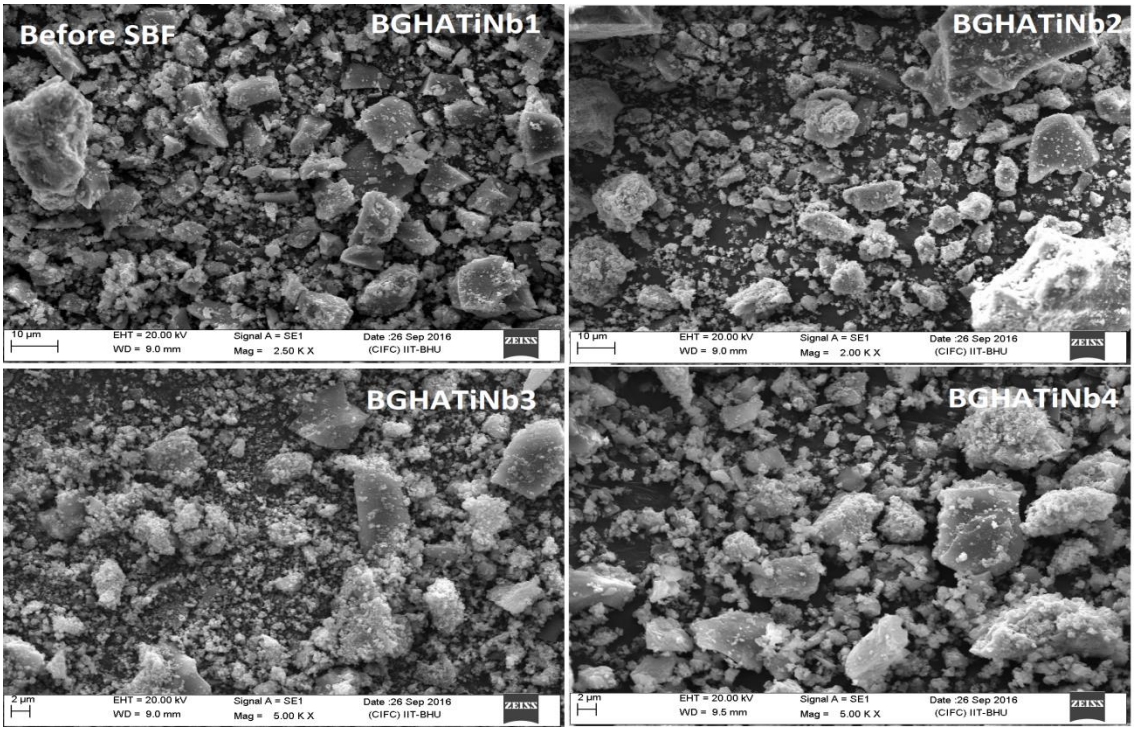

(a)

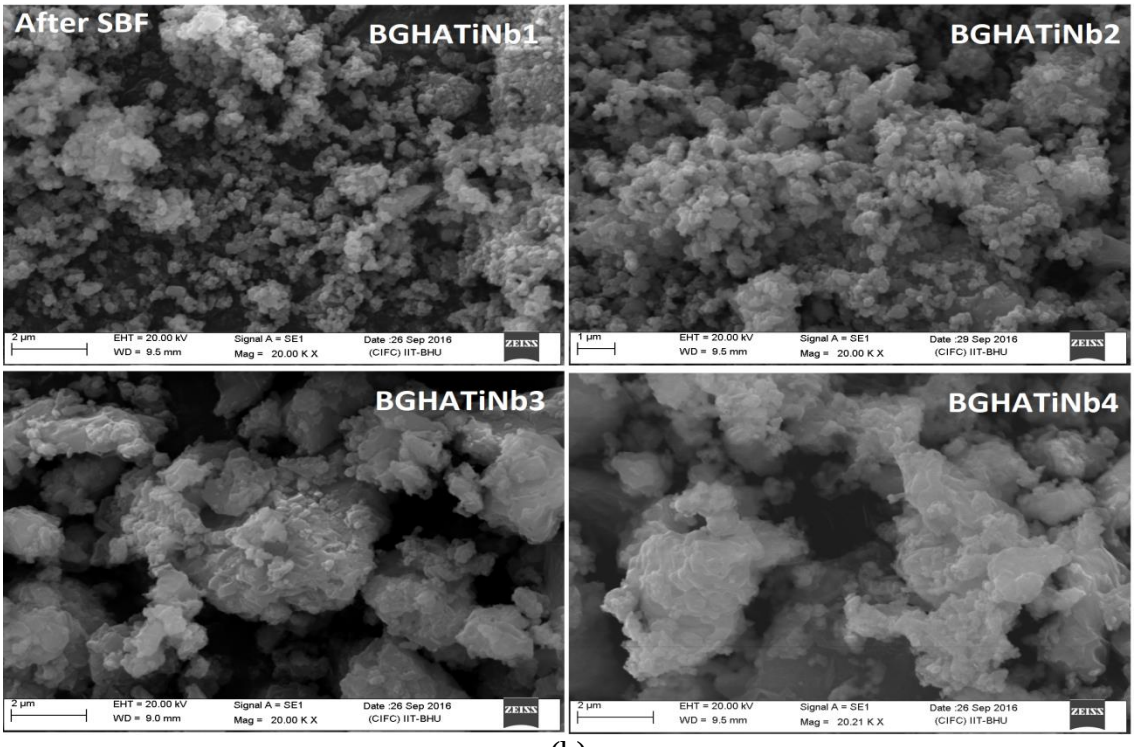

(b)

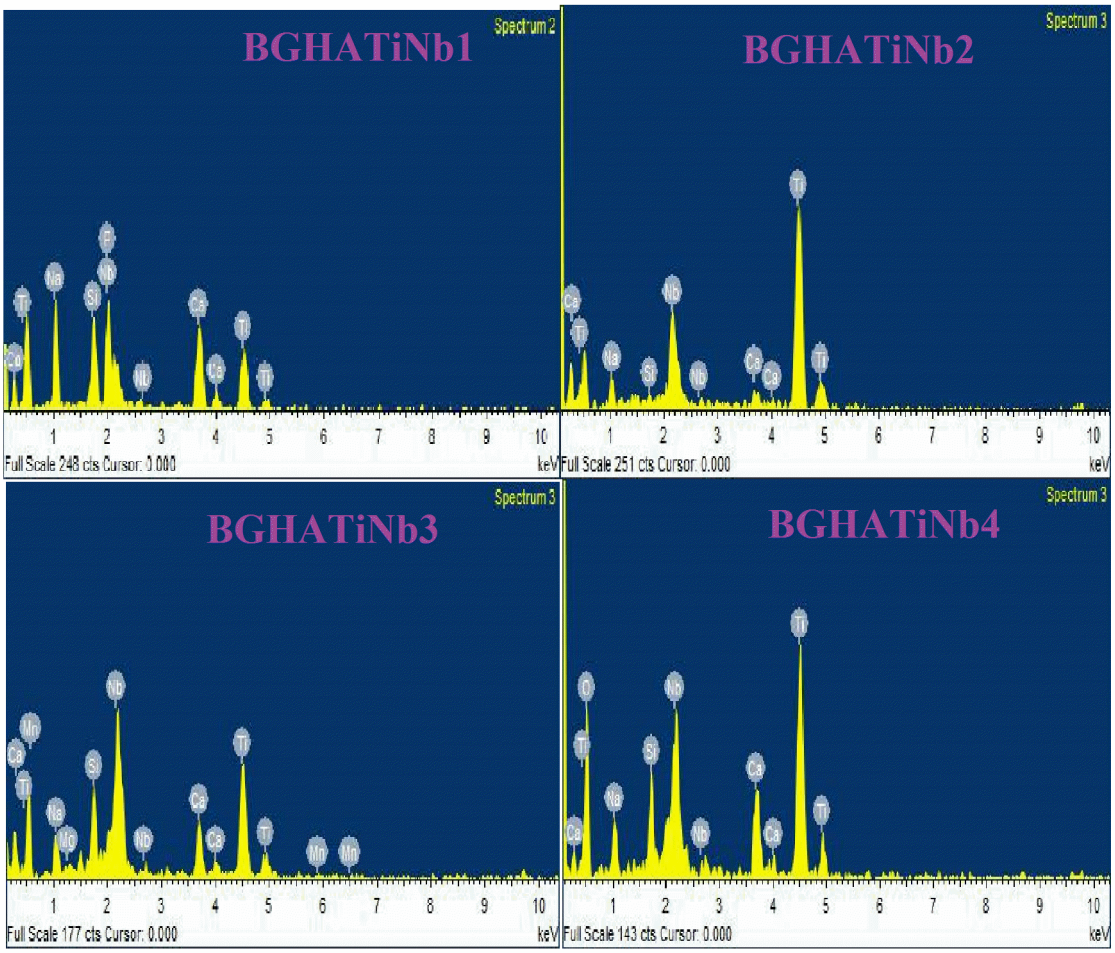

(c)

Figure 7.5 SEM analysis before (a) and after (b) immersion in SBF and EDS (c) of BGHATiNb1, BGHATiNb2, BGHATiNb3, BGHATiNb4 biocomposite sample.

7.3.6 Atomic Force Microscope Analysis

AFM Analysis was carried out by using NTEGRA PRIMA (NT-MDT Russia). The scanning mode is semi contact or tapping mode and scanning speed is 0.5Hz. Fig.7.6 shows AFM analysis where 2-D, 3-D morphology of BGHATiNb4 biocomposite were observed. The topography of the biocomposite substrate indicated that the sample was without any cracks in nature. The surface roughness of the composite was calculated

and the root mean square roughness (Rrms) was found to be 18.6 nm. This biocomposite is expected to facilitate HA growth in vitro [Zinger O et al. 2004].

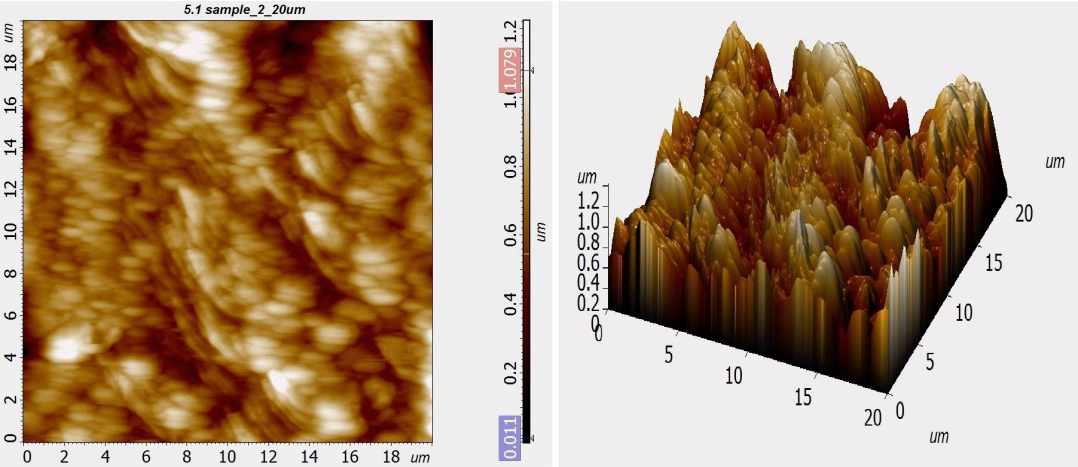

Figure 7.6 Atomic Force Microscope analysis of BGHATiNb4 biocomposite sample.

The portion of peaks of the NbO_6 isolated unit to Nb–O bonding decreased with the increase in the Nb_2O_5 content, the portion of the peak of the NbO_4 tetrahedron bonding increases whereas the portions of the peaks of the NbO_6 chain remain almost constant. Therefore we proposed that the niobium ions do not form NbO_6 as a glass network modifier but NbO_4 function as a glass network former by increasing the Nb_2O_5 content and formed P–O–Nb bonds in the glass. When the Na_2O in the glass is substituted for more than a 25wt% Nb_2O_5 content, the isolated NbO_6 units may aggregate to form a long-chain structure.

7.3.7 Physical and Mechanical Measurement

Compressive strength and density of BGHATiNb1, BGHATiNb2, BGHATiNb3, and BGHATiNb4 biocomposite are shown in Fig.7.7. It was observed that compressive strength of these biocomposite increases with increasing amount of TiO_2, Nb_2O_5 and HA in 45S5 bioglass. The compressive strength of biocomposite is 995, 1220, 1325,

1468MPa and density is 2.44, 2.86, 2.95, 3.24gm/cm^3 respectively. An elastic modulus of biocomposites are increasing from 40.67, 42.57, 45.16, 53.23GPa and yield strength are decreasing from 998, 880, 860, 790MPa respectively.

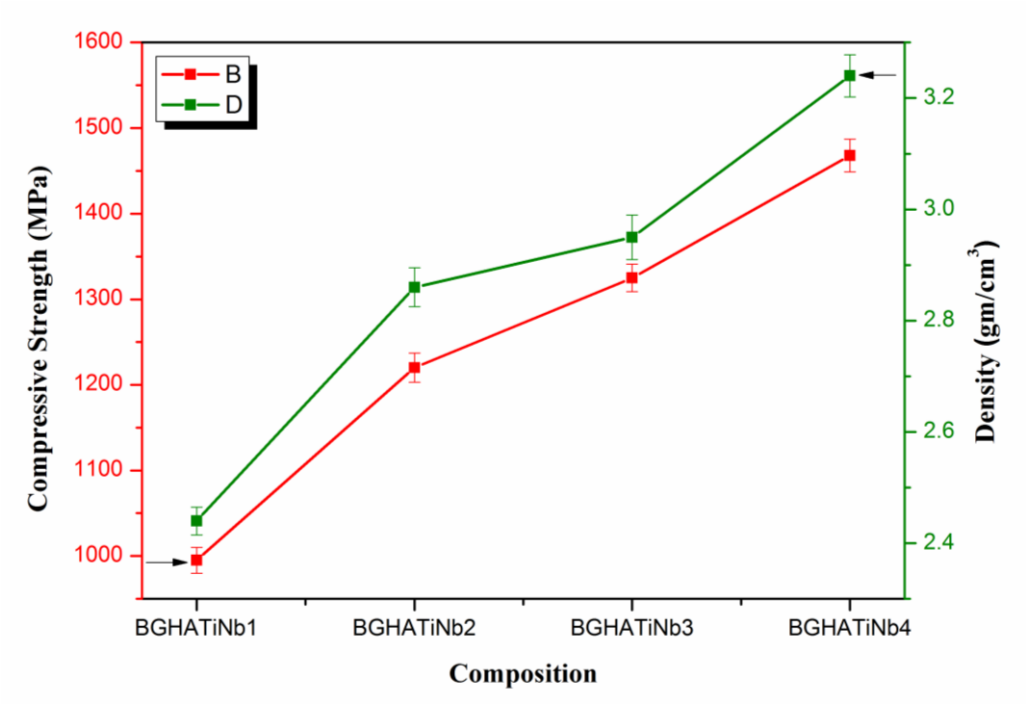

(a)

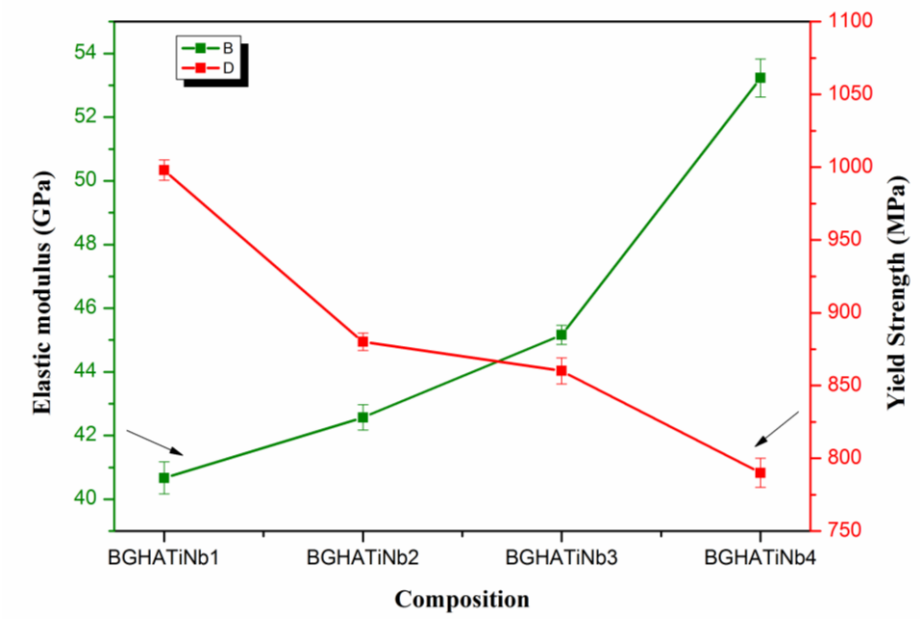

(b)

Figure 7.7 Compressive strength and Elastic modulus of BGHATiNb1, BGHATiNb2, BGHATiNb3 and BGHATiNb4 biocomposite.

7.4 Conclusion

Biocomposite after immersion in simulated body fluid XRD, FTIR spectra, pH behavior, and SEM images indicated the formation of hydroxyl carbonate apatite layer on the surface of biocomposites. Increasing the reinforcement of HA, TiO_2, Nb_2O_5 in base 45S5 bioglass, the value of density, compressive strength and elastic modulus also increases. This study suggested the feasibility of using reinforced BGHATiNb1, BGHATiNb2, BGHATiNb3 and BGHATiNb4 biocomposite as orthopedic implant materials.

7.5 Comparison of mechanical properties of biocomposites

In this thesis comparison of BC, BGHATi biocomposite in Table 7.3 shows mechanical properties of BGHATi biocomposite is increasing with increasing amount of titanium and hydroxyapatite in bioglass. The density of BGHAFeCo sample is more than other four types of biocomposites. Hardness value of BGHATiNb is more than other four types of biocomposites. In Fig. 7.8 shows the comperative study of compressive strength of BGHATiNb is more than BC, BGHATi, BHZ, BGHAFeCo biocomposite.

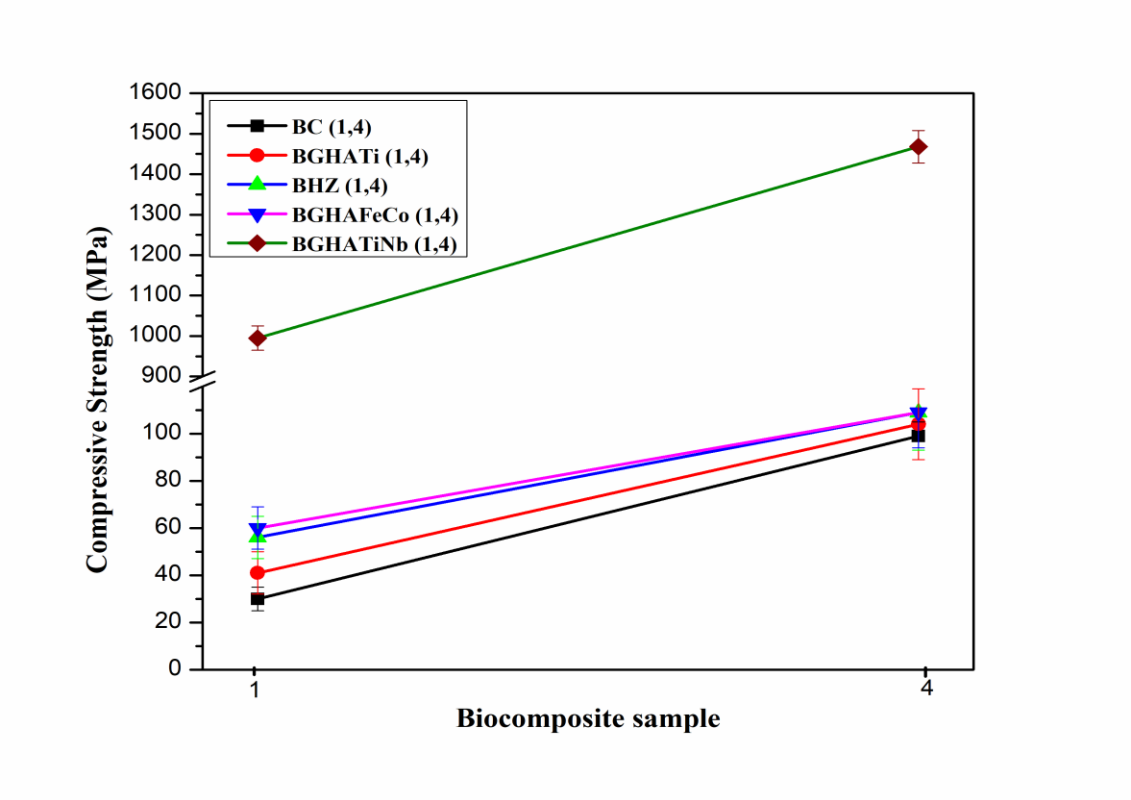

Figure 7.8 Compressive strength of BC(1,4), BGHATi(1,4), BHZ(1,4), BGHAFeCo (1,4) and BGHATiNb(1,4) biocomposites.

Table 7.3: Mechanical properties of BC, BGHATi, BHZ, BGHAFeCo, BGHATiNb biocomposite.

Material	**Density(gm/cm^3)**	**Hardness (HV)**	**Compressive strength [MPa]**
BC (1-4)	2.40-2.45	105-374	30-99
BGHATi (1-4)	2.62-2.82	125-377	41-104
BHZ (1-4)	2.41-3.09	532-712	56-109
BGHAFeCo (1-4)	2.67-2.87	540-612	60-109
BGHATiNb (1-4)	2.44-3.24	612-803	995-1468